Design of a Photonic Bandgap Fiber with Optimized Parameters to Achieve Ultra-Low Confinement Loss

M. Aliramezani* and Sh. Mohammad-Nejad*

Abstract: In this paper, a novel design of all-solid photonic bandgap fiber with ultra-low confinement loss is proposed. The confinement loss is reduced remarkably by managing the number of rods rings, up-doping level, pitch value, and rods diameters. Moreover, the designed PCF shows ultra-flattened dispersion in L- and U-band. Furthermore, a new design, based on introducing of an extra ring of air holes on the outside of the all-solid bandgap structure, is then proposed and characterized. We demonstrate that it significantly reduces the fiber diameter to achieve negligible confinement loss. The validation of the proposed design is carried out by employing a two dimensional finite difference frequency domain with perfectly matched layers.

Keywords: Confinement loss, Dispersion, Finite difference frequency domain, Photonic bandgap fiber, Up-doping.

1 Introduction

In the large family of photonic crystal fibers (PCFs) [1-4], photonic bandgap fibers (PBGFs) are probably the most original ones as the light in these structures is confined in a low index core conversely to all the other fibers. PBGF is an optical fiber in which light is confined to the core by a photonic bandgap of the cladding, instead of the total-internal reflection [2]. Hollow-core PBG fibers with air holes in a glass background, as a hot investigation field, allow low-loss propagation in an empty or gas-filled core, giving the fibers several interesting properties and applications [5]. However, these fibers suffer from some important drawbacks, such as tricky fabrication and splicing to other fibers. Furthermore, surface modes appear in these structures, limiting significantly the fiber properties. Comparing to hollow–core bandgap fiber, all-solid PBGF is better to realize rare-earth-doped amplifier and laser or to fabricate Bragg gratings which are widely used in photonics. Furthermore, these fibers should be easier to fabricate and splice for their elimination of mechanically unstable holey structure.

In all-solid PBGFs, the core is made from a low index area formed by omitting one or several rods [6, 7]. Since the mean core–cladding index contrast is negative, TIR cannot take place, and photonic bandgap effects are the only possible guidance mechanisms.

In PCFs, it is necessary to consider another contribution to the losses, that is the leakage or confinement losses. These are due to the finite number of air-holes which can be made in the fiber cross section. As a consequence, all the PCF guided modes are leaky. For example, in solid-core PCFs light is confined within a core region by the air-holes. Light will move away from the core if the confinement provided by the air-holes is inadequate. This means that it is important to design such aspects of the PCF structure as air hole diameter and hole-to-hole spacing, or pitch, in order to realize low-loss PCFs. In particular, the ratio between the air-hole diameter and the pitch must be designed to be large enough to confine light into the core. On the other hand, a large value of the ratio makes the PCF multi-mode. However, by properly designing the structure, the confinement loss of single-mode PCFs can be reduced to a negligible level [8].

The outline of this paper is the following: in the next section, we describe the numerical method which is used to characterize the fiber structure. In section 3, we propose our design to achieve the desirable characteristics. After that numerical results are discussed and finally a design to reduce the number of doped ring is proposed and analyzed.

2 Theoretical Discussion

Two dimensional finite difference frequency domain (2-D FDFD) is popular and appealing for numerical electromagnetic simulation due to its many merits. The

Iranian Journal of Electrical & Electronic Engineering, 2012.
Paper first received 18 Dec. 2010 and in revised form 10 Apr. 2012.
* The Authors are with the Nanoptronics Research Lab, Department of Electrical Engineering, Iran University of Science and Technology, Tehran , Iran.
E-mails: Maliramezani@iust.ac.ir, Shahramm@iust.ac.ir.

discretization scheme can be derived from the Helmholtz equations [9] or Maxwell's equations [10] directly. Now we use the direct discretization schemes first described for photonic crystal fibers by Zhu et al [10]. Yee's two-dimensional mesh is illustrated in Fig. 1. Note that the transverse fields are tangential to the unit cell boundaries, so the continuity conditions are automatically satisfied. After inserting the equivalent non split-field anisotropic PML (Perfectly Match Layer) [11] in the frequency domain, the curl Maxwell equations are expressed as:

$$\begin{aligned} jk_0 s\varepsilon_r E &= \nabla \times H \\ -jk_0 s\mu_r H &= \nabla \times E \end{aligned} \tag{1}$$

$$s = \begin{bmatrix} \frac{s_y}{s_x} & & \\ & \frac{s_x}{s_y} & \\ & & s_x s_y \end{bmatrix} \tag{2}$$

where μ_r and ε_r are the relative permittivity and permeability of the medium considered, and $k_0=2\pi/\lambda$ is the wave number in free space. For *exp(-jωt)* convention which is used in this paper:

$$s_x = 1-\frac{\sigma_x}{j\omega\varepsilon_0}, s_y = 1-\frac{\sigma_y}{j\omega\varepsilon_0} \tag{3}$$

where σ conductivity the medium considered, and ε_0 is permeability in free space.

In the compact-2D scheme for waveguides, the z-derivatives are replaced by analytical expressions using Eq. (1), and other derivatives are replaced by finite differences in Yee's mesh. Therefore, the curl Eq. (1) can be expressed in matrix form [11]:

$$-jk_0 \begin{bmatrix} \frac{s_y}{s_x}\varepsilon_{rx} & & \\ & \frac{s_x}{s_y}\varepsilon_{ry} & \\ & & s_x s_y \varepsilon_{rz} \end{bmatrix} \begin{bmatrix} E_x \\ E_y \\ E_z \end{bmatrix} = \begin{bmatrix} 0 & -j\beta(I) & V_y \\ j\beta(I) & 0 & -V_x \\ -V_y & V_x & 0 \end{bmatrix} \begin{bmatrix} H_x \\ H_y \\ H_z \end{bmatrix} \tag{4-a}$$

$$jk_0 \begin{bmatrix} \frac{s_y}{s_x}\mu_{rx} & & \\ & \frac{s_x}{s_y}\mu_{ry} & \\ & & s_x s_y \mu_{rz} \end{bmatrix} \begin{bmatrix} H_x \\ H_y \\ H_z \end{bmatrix} = \begin{bmatrix} 0 & -j\beta(I) & U_y \\ j\beta(I) & 0 & -U_x \\ -U_y & U_x & 0 \end{bmatrix} \begin{bmatrix} E_x \\ E_y \\ E_z \end{bmatrix} \tag{4-b}$$

where the U and V are sparse matrices which are obtained in the same way as in [11, 12] and I is an identity matrix.

Eliminating the longitudinal magnetic and electric fields, the eigenvalue matrix equation in terms of transverse magnetic fields and transverse electric fields can be obtained as:

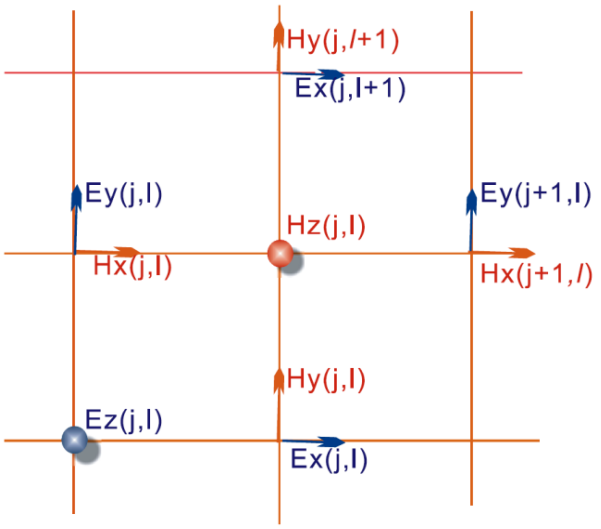

Fig. 1 Unit cell in Yee's 2D-FDFD mesh.

$$\begin{bmatrix} Q_{xx} & Q_{xy} \\ Q_{yx} & Q_{yy} \end{bmatrix} \begin{bmatrix} H_x \\ H_y \end{bmatrix} = \beta^2 \begin{bmatrix} H_x \\ H_y \end{bmatrix} \tag{5-a}$$

and

$$\begin{bmatrix} P_{xx} & P_{xy} \\ P_{yx} & P_{yy} \end{bmatrix} \begin{bmatrix} E_x \\ E_y \end{bmatrix} = \beta^2 \begin{bmatrix} E_x \\ E_y \end{bmatrix} \tag{5-b}$$

where the Q and P are highly sparse coefficient matrices [12]. The order and the nonzero elements in them are reduced and effectively stored in sparse format, so the computation efficiency is improved greatly. The complex propagation constant β and the transversal magnetic or electric field distribution can be solved out quickly and accurately by a sparse matrix solver [13].

The dispersion characteristic is obtained by the following equation [14]:

$$D(\lambda) = -\frac{\lambda}{c}\frac{d^2 n_{eff}}{d\lambda^2} \tag{6}$$

where c is the velocity of light in a vacuum and $n_{eff}=\beta/k0$ is effective index. When the hole diameter to pitch ratio is very small and the hole pitch is large, the dispersion curve is close to the material dispersion of pure silica. As the air-hole diameter is increased, the influence of waveguide dispersion becomes stronger.

Due to the finite number of air-holes which can be made in the fiber cross section, all the PCF guided modes are leaky. Under this circumstance, the effective index is a complex value and the confinement loss proportionate to imaginary part of β and is calculated by using [14]:

$$L_c = 8.686 \times \mathrm{Im}[\beta] \tag{7}$$

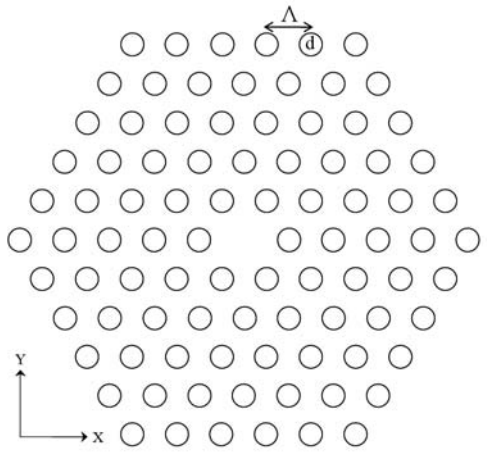

Fig. 2 Cross sectional view of the test case PCF [15].

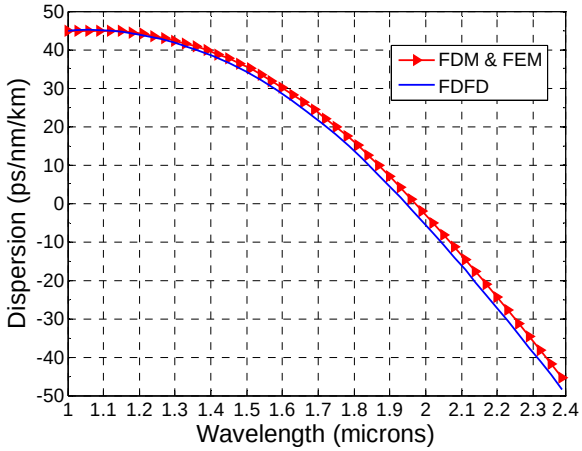

Fig. 3 Dispersion curve of the test case PCF as a function of wavelength. *d=1 μm, Λ=2.3 μm*.

For validation of our simulations with the FDFD, simulated results are compared with results of [15] and [16] which are used Finite Element Method (FEM) and vector Finite Difference Method (FDM) respectively. The cross-sectional view of the test case PCF is shown in Fig. 2. Parameters of the PCF are *d=1 μm*, *Λ= 2.3 μm*, $n_{silica}=1.44$, and $n_{air}=1$. Fig. 3 illustrates the dispersion characteristic of the PCF by using FEM [15], FDM [16], and FDFD. According to Fig. 3, the simulated results by the FDFD are in excellent agreement with the FDM and the FEM simulation.

3 Design

The proposed all-solid PBGF is formed by up-doped rods around a core that is made from omission of seven rods. As a result, the all-solid PBGF structure imposes photonic bandgap guidance as the dominant guidance mechanism. The cross-section of the proposed all-solid PBGF is shown in Fig. 4. As it can be seen, the all-solid PBGF has a triangular lattice of rods in cladding.

The all-solid PBGF geometrical parameters are included: two different rod diameters, d_1 for the three inner rings and d_2 for the rest of rings, and pitch (Λ) which is the center-to-center spacing between the nearest rods. The background silica index is assumed to be 1.45 and the index of the rod corresponds to up-doped silica. In this paper, confinement loss is reduced to negligible level by managing number of the cladding rings (N_r), up-doping level, pitch value, and rods diameters.

The mode field distribution of the proposed all-solid PBGF is depicted in Fig. 5. It is evident that the guided mode is well confined.

In this article, $d_1=d_2=6$ *μm*, and $\Lambda=8$ *μm* are chosen as the basic geometrical parameters. One should note that up-doping level (or the index contrast of the two materials) is defined by following equation.

$$\Delta n\% = (\text{rods index} - \text{background index})/100 \quad (8)$$

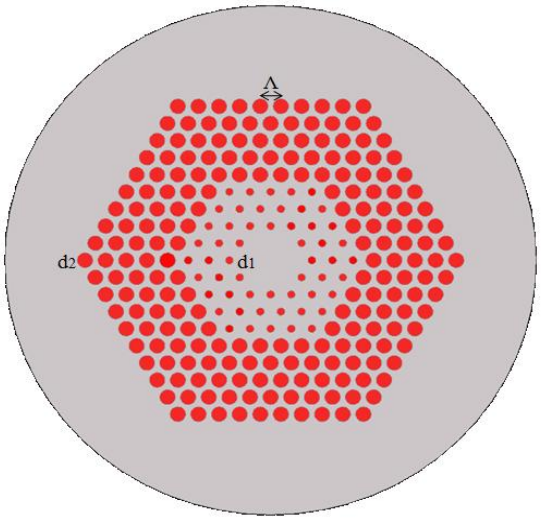

Fig.4 Cross-sectional view of the PBGF.

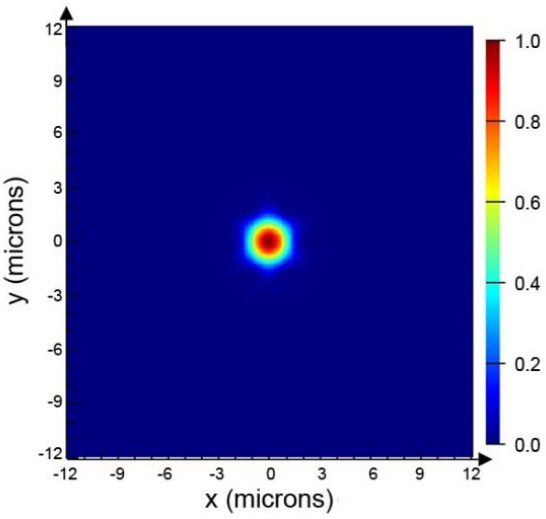

Fig. 5 Transversal field intensity distribution at a wavelength of $\lambda = 1.55$ *μm* for the fundamental guiding mode. $d_1=d_2=6$ *μm* and *Λ=8 μm*.

4 Numerical Result

Table 1 shows confinement loss variation with number of rings increasing. As we expected, the larger number of rods rings provides the more confined guided mode and result in lower confinement loss. Moreover, Table 1 shows that 12 rings are large enough to achieve negligible confinement loss. Although the confinement loss can be reduced simply by increasing the number of the rings, this will result in a thicker fiber diameter.

We are also interested in the influence of up-doping level (Δn) on the confinement loss. Table 2 demonstrates confinement loss behavior with increment of up-doping level. Surprisingly, the dependence of confinement loss on doping level is found weaker than number of rods rings dependence (see Tables 1 and 2). As Table 2 depicts, confinement loss can be reduced by increasing the up-doping level.

It can be also seen from Table 3, where confinement loss with different Λ is depicted, the pitch has important influence on confinement loss and affect it remarkably. It is due to that increment of Λ provides a larger core area. As a result, more light is guided through core and confinement loss decreases remarkably. It can be also inferred: achieving low-loss for a small-core fiber with an all-solid PBGF design is difficult.

Table 4 shows how the confinement loss is reduced as d_1 increases. It should be pointed that by employing simulation, it is understood that d_1 has a major impact on confinement loss in comparison with d_2.

Table 1 Confinement loss at a wavelength of *1.55 μm* for different number of cladding rings. $d_1= d_2=6\ \mu m$, $\Lambda=8\ \mu m$, and $\Delta n =2\%$

N_r	Confinement loss (*dB/km*)
8	892.61
10	1.007
12	2.9923×10^{-9}
14	8.0090×10^{-10}
16	3.6378×10^{-10}
18	-4.8170×10^{-11}

Table 2 Confinement loss at a wavelength of *1.55 μm* for different up-doping level (Δn). $d_1=d_2=6\ \mu m$, $\Lambda=8\ \mu m$, and $N_r=14$.

Δn	Confinement loss (*dB/km*)
1%	1.2127×10^{-7}
1.5%	1.1788×10^{-9}
2%	8.0090×10^{-10}
2.5%	1.3150×10^{-10}
3%	5.6310×10^{-12}

Table 3 Confinement loss at a wavelength of *1.55 μm* for different Λ. $(d_1=d_2)/\Lambda =6/8$, $N_r=14$ and $\Delta n=2\%$

Λ	Confinement loss (*dB/km*)
6	1.0709×10^{-1}
7	2.0048×10^{-4}
8	8.0090×10^{-10}
9	4.1547×10^{-10}
10	5.7224×10^{-11}

Table 4 Confinement loss at a wavelength of *1.55 μm* for different d_1. $d_2=6\ \mu m$, $\Lambda=8\ \mu m$, $N_r=14$ and $\Delta n=2\%$

d_1	Confinement loss (*dB/km*)
4	21.663
5	1.8079×10^{-4}
6	8.0090×10^{-10}
7	-1.4574×10^{-9}
7.8	-2.1102×10^{-9}

Fig. 6 demonstrates dispersion as a function of wavelength in the third telecommunication window; (*1.55 μm* to *1.7 μm*) with different d_1 ($d_2 =6\mu m$, $\Lambda=8\mu m$, $N_r=14$ and $\Delta n=2\%$). According to Fig. 6, dispersion and dispersion variation are decreased with d_1. Thus, it is believed; more flattened dispersion can be attainable by using larger Λ and d_1. But it leads to thicker fiber consequently.

Figs. 7 and 8 show dispersion and confinement characteristics of the proposed all-solid PBGF versus wavelength when $d_1 =7.8\ \mu m$, $d_2=6\ \mu m$, $\Lambda=8\ \mu m$, $N_r=14$ and $\Delta n=2\%$. In comparison with other designs, the proposed design illustrates highly better characteristics. For instance, the introduced deign by [17] can just achieve confinement loss of 10^{-6}, however, the proposed design gain ultra-low confinement loss of 10^{-10}. Furthermore, Based on Fig. 8, ultra-flattened dispersion slope of 0.0074 (*ps/nm²/km*) and 0.0079 (*ps/nm²/km*) can be obtained in L-band (*1.565 μm* to *1.625 μm*) and U-band (*1.625 μm* to *1.675 μm*) respectively.

As we know, one of the popular structures for all-solid PBGF is triangular photonic crystal-honeycomb photonic crystal (TPC-HPC). Fig. 9 demonstrates the cross-section of all-solid PBGF with TPC-HPC structure. In comparison with triangular structure, TPC-HPC shows a little higher confinement loss (see Figs. 10 and 6). This mainly is related to that; TPC-HPC structure has a lower cladding-core contrast, because of omitting several rods from its cladding.

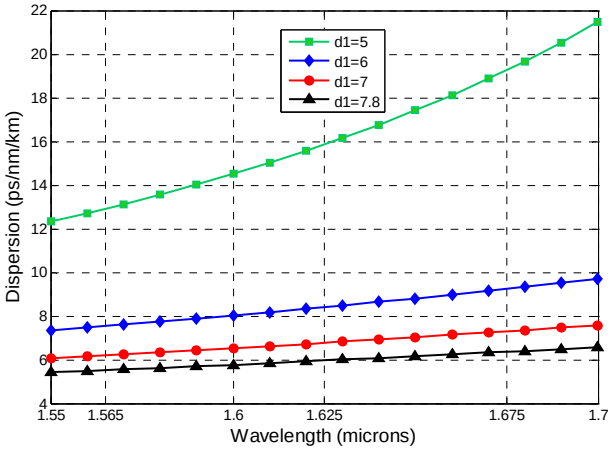

Fig. 6 Dispersion characteristic of the PBGF with different d_1. d_2 *=6μm,* Λ*=8μm,* N_r*=14* and Δn*=2%.*

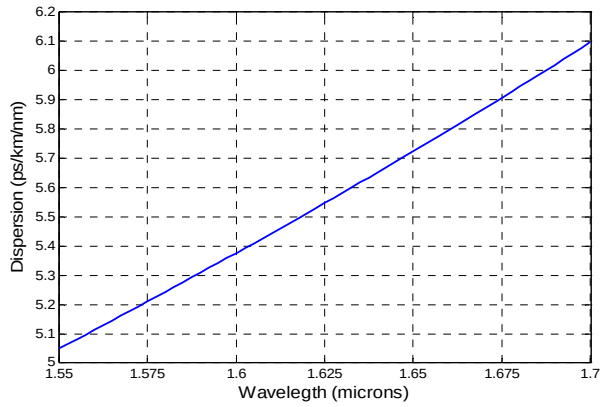

Fig. 7 Dispersion characteristic of the PBGF. d_1*=7.8 μm,* d_2 *=6 μm,* Λ*=8μm,* N_r*=14* and Δn*=2%.*

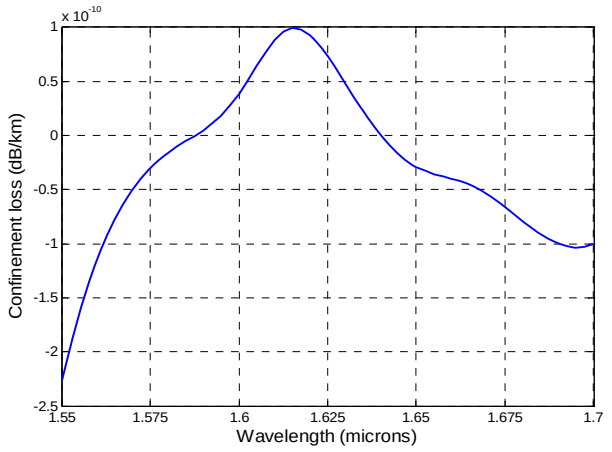

Fig. 8 Confinement loss characteristic of the PBGF. d_1*=7.8 μm,* d_2*=6μm,* Λ*=8μm,* N_r*=14* and Δn*=2%.*

5 PBGF with an Extra Air-Hole

In this section we propose an alternative design to reduction of the number of doped rings. It is based on using an extra air-hole ring to help the confinement of the core mode. The cross-section of the designed all-solid PBGF with an extra air-hole ring is shown in Fig. 11.

In this design, we introduce another geometric parameter: d_a, which is the air-hole diameter of the seventh ring. As can be seen from Fig. 12, ultra-low confinement loss can be achieved by using only 7 rings. It should be noted that confinement loss of *892.61 dB/km* at a wavelength of *1.55 μm* is obtained by using Fig. 5 design and 8 rods rings (see Table 1).

It is noteworthy that the holey ring will act as a low index layer compared to the high index doped microstructured region. Thus, any cladding modes with effective index higher than n_{FSM} will also benefit from the confinement offered by the depressed cladding region. In particular, all the cladding modes with effective index lower than n_{silica} were leaky in our previous design, whereas some of these modes will be allowed to propagate along the fiber with relatively low losses. Because of the loss reduction of these unwanted

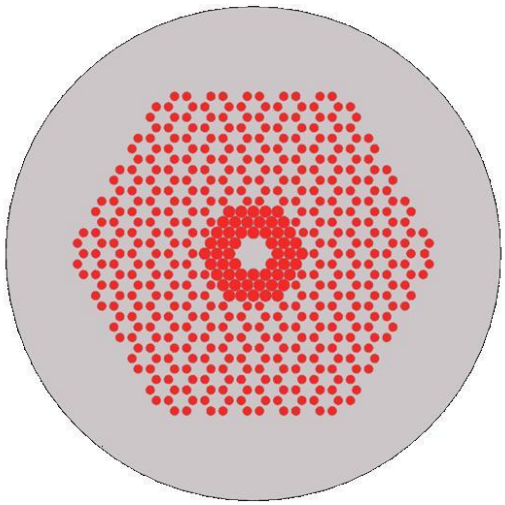

Fig. 9 Cross-sectional view of the PBGF with TPC-HPC structure.

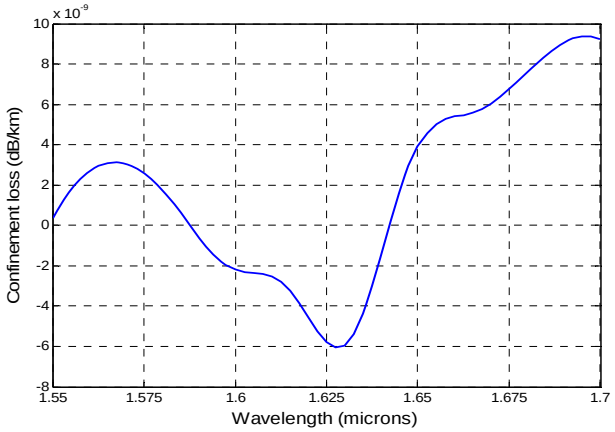

Fig. 10 Confinement loss characteristic of the PBGF with TPC-HPC structure. d_1*=7.8 μm,* d_2 *=6μm,* Λ*=8μm,* N_r*=14* and Δn*=2%.*

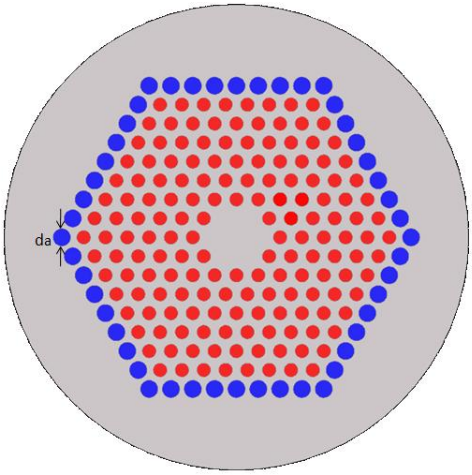

Fig. 11 Cross-sectional view of the PBGF with an extra air-hole ring.

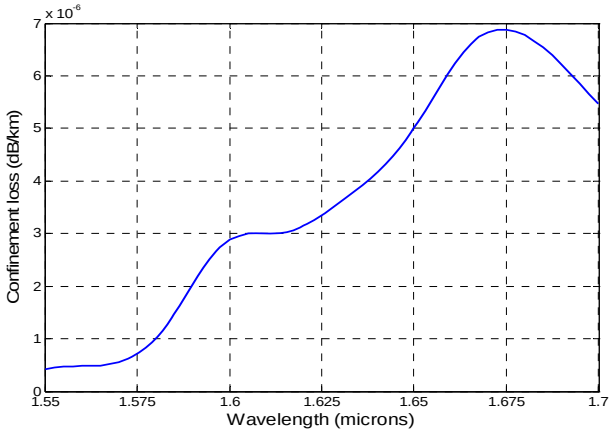

Fig. 12 Confinement loss characteristic of the PBGF with an extra air-hole ring. $d_1=d_2=6\ \mu m$, $d_a=7.8$, $\Lambda=8\ \mu m$, $N_r=7$ and $\Delta n=2\%$.

Table 5 Confinement loss at a wavelength of 1.55 µm for different d_a. $d_1= d_2=6\ \mu m$, $N_r=7$, $\Delta n=2\%$, and $\Lambda=8\ \mu m$.

d_a	Confinement loss (*dB/km*)
4	9.2687
5	3.3405×10^{-2}
6	6.9670×10^{-4}
7	3.7835×10-6
7.8	4.3307×10^{-7}

modes, one has to avoid realizing a depressed cladding with a too low refractive index and with a too large section. This is also why we limit ourselves to only one ring of air-hole.

Table 5 illustrates the confinement loss values of the PBGF with an extra air-hole ring as d_a increases. In accordance with our expectation, because of lower loss properties of air, the confinement loss decreases with increasing of d_a [18, 19].

6 Conclusions

In this article, an all-solid PBGF with ultra-low confinement loss and ultra-flattened dispersion is proposed. The all-solid PBGF presents negligible confinement loss of -2.1102×10^{-9} (*dB/km*) at a wavelength of 1.55µm. Moreover, the proposed PCF shows ultra-flattened dispersion of $\Delta D=0.445$ (*ps/nm/km*) and $\Delta D=0.399$ (*ps/nm/km*) in L-band (*1.565 µm* to *1.625 µm*) and U-band (*1.625 µm* to *1.675 µm*) respectively. Furthermore, we proposed a novel design consisting in the addition of a ring of air holes around the all-solid PBGF. The design has the important benefit to reduce significantly the fiber diameter. This paper foreshows the ultra-low confinement loss and ultra-flattened dispersion capability of all-solid PBGF, which may be used in nonlinear application or to raise the radiation efficiency of rare earth element doped fibers.

References

[1] Bouwmans G., Bigot L., Y Quiquempois., Lopez F., Provino L. and Douay M., "Fabrication and characterization of an all-solid 2D photonic bandgap fiber with a low-loss region (< 20 dB/km) around 1550 nm", *Opt. Express*, No. 13, pp. 8452-8459, 2005.

[2] Knight J. C., "Photonic crystal fibres", *Nature*, No. 424, pp. 847-851, 2003.

[3] Bjarklev A., Broeng J. and Bjarklev A. S., "*Photonic Crystal Fibres*" , Kluwer Academic Publishers, Boston, 2003.

[4] Belardi W., Bouwmans G., Provino L. and Douay M., "Form-induced birefringence in elliptical hollow photonic crystal fiber with large mode area", *IEEE J. Quantum Electron*. No. 41, pp. 1558-1564, 2005.

[5] Fink Y., Ripin D. J., Fan S. H., Chen C. P., Joannopoulos J. D. and Thomas E. L., "Guiding optical light in air using an all-dielectric structure", *IEEE J. Lightwave Technol*. No. 17, pp. 2039–2041, 1999.

[6] Stone J. M., Pearce G. J., Luan F., Birks T. A., Knight J. C., George A. K. and Bird D. M., "An improved photonic bandgap fiber based on an array of rings", *Opt. Express*, No. 14, pp. 6291-6296, 2006.

[7] Argyros A., Birks T. A., Leon-Sava S. G., Cordeiro C. M. B. and Russell, P. St. J., "Guidance properties of low contrast photonic bandgap fibers", *Opt. Express*, No.7, pp. 2503–2511, 2005.

[8] Poli F., Cucinotta A. and Selleri S., "Photonic crstal fibers: properties and applications", *Springer*, pp. 38-41, 2007.

[9] Varshney K., Saitoh K. and Koshiba M., "Novel design for dispersion compensating photonic

crystal fiber raman amplifier", *IEEE photonics technology letters*, Vol. 17, No. 10, Oct. 2005.

[10] Nielsen L., Qian Y., Palsottir B., Gaarde P., Dyrbolv S. and Beng T., "Module for simultaneous C+L-band dispersion compensation and Raman amplification," *Proceeding of OFC*, Anaheim, CA, pp. 65–66, Mar. 2002.

[11] Lusse P., Stuwe P., Schule J. and Unger H. G., "Stability properties of 3-D vectorial and semivectorial BPMs utilizing a multi-grid equation solver", *IEEE J. Lightwave Technol*., No. 12, pp. 487–94, 1994.

[12] Li L. and Mao J., "An improved compact 2-D finite-difference frequency-domain method for guided wave structures", *IEEE Microw. Wireless Compon. Lett*., No. 13, pp.520–2, 2003.

[13] Saitoh K. and Koshiba M., "Numerical modeling of photonic crystal fibers," *Lightwave Technology*, Vol. 23, No. 11, pp. 3580-3590, 2005.

[14] Abdur Razzak S. M., Namihira Y., Begum F., Kaijage S., Hoang Hai N. and Zou N., "Design of a decagonal photonic crystal fiber for ultra-flattened chromatic dispersion", *IEICE Trans. Electron*, Vol. E90–C, No. 11, pp. 2141-2145, Nov. 2007.

[15] Koshiba M., "Full vector analysis of photonic crystal fibers using the finite element method", *IEICE Electron*, Vol. E85-C, No. 4, pp. 881–888, 2002.

[16] Shen L. P., Huang W. P. and Jian S., "Design of Photonic Crystal Fibers for Dispersion-Related Applications", *Journal of lightwave thechnology*, Vol. 21, No. 7, pp. 1644-1651, July 2003.

[17] Ren G., Shum P., Zhang L., Yan M., Yu X., Tong W. and Luo J., "Design of All-Solid Bandgap Fiber With Improved Confinement and Bend Losses", *IEEE Photonics Technology Letters*, Vol. 18, No. 24, Dec. 15, 2006.

[18] Aliramezani M., Mohammad Nejad Sh., "Numerical analysis and optimization of a dual-concentric-core photonic crystal fiber for broadband dispersion compensation", *Journal of Optics & Laser Technology*, Vol. 42, pp. 1209–1217, 2010.

[19] Mohammad Nejad Sh., Aliramezani M. and Pourmahyabadi M., "Novel Design of an Octagonal Photonic Crystal Fiber with Ultra Flattened Dispersion and Ultra-Low Loss", *Broadband Communications, Information Technology & Biomedical Applications Conference (BroadCom' 08)* , pp. 221–226, 2008.

Mohammad Aliramezani was born on June 15, in Tehran, 1985. He received the B.Sc. degree in Electrical Engineering from Razi University, Kermanshah, Iran, in 2006 and M.S. degree in Electrical Engineering from Iran university of Science and Technology, Tehran, Iran, in 2008. His research interests include semiconductor devices, optoelectronics, electronic devices, optical fiber telecommunication, and lasers.

Shahram Mohammad Nejad received his B.Sc. in Electrical Engineering from University of Houston, Houston, USA, in 1981 and M.S. and Ph.D. degrees in Semiconductor Material Growth and Lasers from Shizuoka University, Shizuoka, Japan, in 1990 and 1993, respectively. Professor Mohammad Nejad invented the PdSrS laser for the first time in 1992. He has published over 80 scientific papers and books. Currently, he is the Head of Electrical Engineering Department, Iran University of Science and Technology, Tehran, Iran. Also, he is a scientific committee member of Iranian Conference on Electrical Engineering (ICEE) and also Iranian Conference on Optics & Photonics, member of Institute of Engineering and Technology (IET) and an IETCEng. His research interests include semiconductor material growth, quantum electronics, semiconductor devices, optoelectronics, electronic devices and lasers.